Journal of Pharmaceutical Sciences 106 (2017) 2115-2122

Contents lists available at ScienceDirect

Journal of Pharmaceutical Sciences

journal homepage: www.jpharmsci.org

Pharmaceutical Nanotechnology

Paclitaxel-Loaded Magnetic Nanoparticles: Synthesis, Characterization, and Application in Targeting

Jilai Tian [1, 2], Caiyun Yan [1], Kunliang Liu [1, 2], Juan Tao [1, 3], Zhenchao Guo [1], Jianping Liu [3], Yu Zhang [1, 2], Fei Xiong [1, 2, *], Ning Gu [1, 2, *]

[1] State Key Laboratory of Bioelectronics, Jiangsu Key Laboratory for Biomaterials and Devices, School of Biological Sciences & Medical Engineering, Southeast University, Nanjing, China
[2] Collaborative Innovation Center of Suzhou Nano-Science and Technology, Suzhou Key Laboratory of Biomaterials and Technologies, Suzhou, China
[3] Department of Pharmaceutics, China Pharmaceutical University, Nanjing, China

ARTICLE INFO

Article history:
Received 2 October 2016
Revised 14 March 2017
Accepted 13 April 2017
Available online 26 April 2017

Keywords:
PEG
circulation lifetime
target ability
magnetic nanoparticles
paclitaxel

ABSTRACT

Iron oxide magnetic nanoparticles (MNPs) are good candidates to implement fluid therapy in critical patients in clinic integrated system. Herein, we synthesized paclitaxel (PTX)-loaded MNPs modified with methoxy polyethylene glycol (PEG)-lysine-oleic acid$_2$ (PTX-MNPs-PLO), which is expected to act as a magnetic resonance imaging (MRI) contrast agent and meanwhile for cancer therapy. MNPs were synthesized by thermal decomposition. Dialysis method was applied to prepare PTX-MNPs-PLO with 3 different PEG molecular weights (1000, 2000, and 4000 Da), which were subsequently freeze-dried into powders. PTX-MNPs-PLO was characterized by transmission electron microscope, scanning electron microscope, thermogravimetric analysis, vibrating sample magnetometer, and MRI. What is more is that pharmacokinetics and distribution *in vivo* were processed, the results of which exhibited that PTX-MNPs-PLO$_{2000}$ had the longer circulation lifetime compared with Taxol, PTX-MNPs-PLO$_{1000}$, and PTX-MNPs-PLO$_{4000}$. Results of magnetic targeting in kidneys suggested that deep buried or ultrasmall magnet is likely to be more preferable. PTX-MNPs-PLO$_{2000}$ holds great promise in the application of magnetic accumulation, target drug delivery, and thermal therapy.

Introduction

Owing to the size-dependent superparamagnetism, inoffensive toxicity profile, and biocompatibility with cells and tissues, iron oxide magnetic nanoparticles (MNPs) have gained increasing attention and manifested the great potential in various biomedical applications that involved targeted drug delivery,[1] magnetic resonance imaging (MRI) contrast enhancement,[2] and hyperthermia.[3,4] MNPs can also be used as carriers loading fluorescent molecules, genes, or drugs, resulting in imaging, chemotherapy, photodynamic therapy, and so on.[5] Therefore, MNPs can combine multiple functions into one single system, then realize integration of tumor diagnosis and therapy, further providing new insights for personalized medicine development.

For example, paclitaxel (PTX), an excellent antitumor compound found in nature, is always used as a model cargo to evaluate the superiority of drug carrier.[6] First, the natural poor solubility of PTX hinders its clinical applications. Second, Cremophor EL® used in the commercial preparation (Taxol) has been demonstrated causing severe anaphylactic response because of stimulating release of histamine.[7] Although PTX is also clinically available in a Cremphor EL®-free formulation under the trade name of Abraxane™, PTX is always selected to be designed in an advanced delivery system to lower the side effects and enlarge its biomedical applications.

However, the circulating particles *in vivo*, such as MNPs, are always cleared rapidly as exogenous substances by the mononuclear phagocyte system (MPS), dramatically limiting their biologic applications. Therefore, strategies to modify MNPs are needed to avoid adsorption of plasma protein and circumvent the uptake by MPS. In general, methods of minimizing the size of nanoparticles (NPs) or enhancing the hydrophilic properties of particle's surfaces are always involved to escape from this nonspecific uptake.[8]

Sufficient reports have demonstrated that the technology of polyethylene glycol (PEG) can provide the hydrophilic particle surface.[9] PEG is one of the most investigated biocompatible,

Conflicts of interest: The authors declare no conflict of interest.

* *Correspondence to:* Fei Xiong (Telephone: +86-25-83272476; Fax: +86-25-83272460) and Ning Gu (Telephone/Fax: +86-25-83272460).
E-mail addresses: xiongfei@seu.edu.cn (F. Xiong), guning@seu.edu.cn (N. Gu).

http://dx.doi.org/10.1016/j.xphs.2017.04.023
0022-3549/

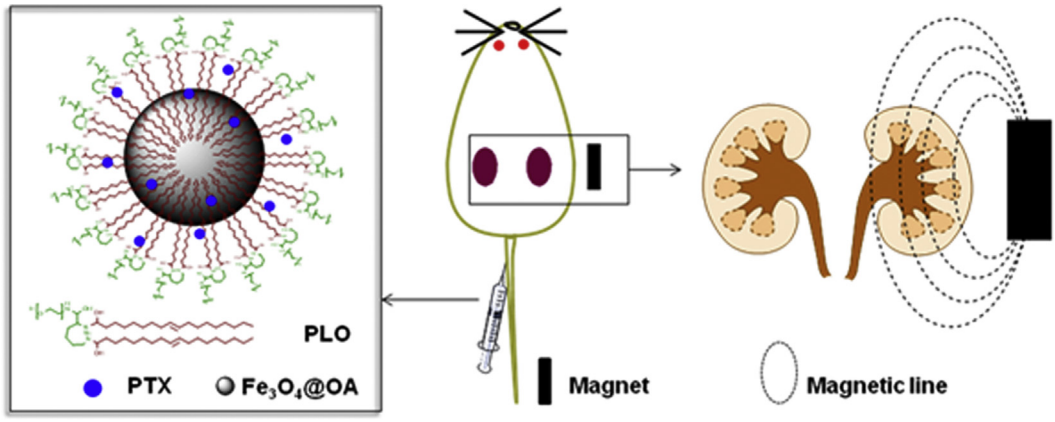

Figure 1. Schematic of PTX-loaded Fe_3O_4@OA modified by PLO and its kidney targeting application.

nontoxic, and hydrophilic polymers, able to modify the surface of carriers, such as liposomes and NPs.[10] It has been widely confirmed that PEGylation of MNPs has potential capability to lower the uptake of MPS and meanwhile prolong the circulating time *in vivo*.[11] Brighter, that the amount of PEG-modified MNPs taken up by the macrophage cells is much lower than that of unmodified MNPs is revealed in most reports. But MNPs coated with different molecular-weight PEGs are seldom investigated in animal level.

In our previous study, PEGs with molecular weight of 1000, 2000, and 4000 Da are selected to synthesize the methoxy PEG (mPEG)-lysine-oleic acid $(OA)_2$ (PLO)[12] and are then used as the coating materials of MNPs in the present study. OA is desired to link the MNPs and PEG, where also, position the hydrophobic PTX. Thus, the aim of this work is to synthesize and characterize PTX-loaded MNPs modified by PLO (PTX-MNPs-PLO). Through the comparison study of performance *in vitro*, and pharmacokinetics *in vivo* of PTX-MNPs-PLO_{1000}, PTX-MNPs-PLO_{2000}, PTX-MNPs-PLO_{4000}, and Taxol, the optimized molecular weight of PLO was obtained. Furthermore, the potential application of magnetic targeting, such as kidney targeting, was investigated and discussed. Figure 1 shows the desired structure of PTX-MNPs-PLO and schematically the exploration of kidney targeting application.

Materials and Methods

Materials

PTX was purchased from Taihua Original Biopharmacy Company, Ltd. PLO_{1000}, PLO_{2000}, and PLO_{4000} were synthesized according to our previous work.[13] Taxol (6 mg/mL) was obtained from Yangtze River Pharmaceutical Group Jiangsu Pharmaceutical Trading Company, Ltd. (Taizhou, China). The other chemicals were analytical reagents and purchased from Sinopharm Chemical Reagent Company, Ltd. The used external magnet made of $Nd_2Fe_{14}B$ was purchased from Shanghai Yici Company, Ltd. (shape, cuboid; size, 40 × 20 × 10 mm; maximum magnetic energy product, 40 MGOe; coercive force, 11.9 KOe; and residual induction, 13.4 kg).

Animals

Clean Sprague-Dawley rats (200 ± 10 g) and male Sprague-Dawley mice (15-20 g) were provided by Laboratory Animals Center of Southeast University (Nanjing, China). Animal experiments were performed via a protocol approved by the Institutional Animal Care and Use Committee of Southeast University.

Preparation of PTX-MNPs-PLO

OA-coated Fe_3O_4 NPs were synthesized by thermal decomposition.[14] Briefly, $FeCl_3 \cdot 6H_2O$ and OA were dissolved in methanol. About 4.8 g of sodium hydroxide (dissolved in methanol) was then added while stirring. When the reaction was completed, the brown deposition was washed with methanol and then dried under vacuum. The resulted iron (Fe) oleate solid was dissolved in 1-octadecene at 70°C and stored at room temperature. About 5.7 g of OA was mixed with aforementioned stock solution containing 36 g of Fe oleate. Under a nitrogen (N_2) atmosphere, the mixture was heated from room temperature at a constant heating rate of 3.3°C/min to 320°C and kept for 30 min. After that, the obtained solution was cooled and precipitated by the addition of ethanol. The precipitates were centrifugated and then dispersed in *n*-hexane and reserved at room temperature.

Dialysis was applied to prepare PTX-MNPs-PLO.[15] Briefly, PLO and PTX were added to the solution of MNPs in tetrahydrofuran (THF). The mixture was dropped through a syringe with pinhead into distilled water under agitation and followed by intermittently probe ultrasonic (Mettler, Greifensee, Switzerland) to form emulsion. The organic solvent was eliminated by dialysis for 24 h. Finally, the ultimate product was subjected to lyophilization to be powders. Different molecular weights of PLO were used in parallel to prepare PTX-MNPs-PLO.

Lyophilization and Resuspension

The aforementioned obtained product was subjected to lyophilization, and mannitol was selected as the freeze-dried protective

Table 1
Effect of Different Amounts of Mannitol on PTX-MNPs

Mannitol (w/v) (%)	Appearance and Reconstitution	Leaking Rate (Fe, %)	Leaking Rate (PTX, %)	Particle Size (nm)
0	Cotton, easy	1.2	5.1	69.1 ± 0.2
1	Brown cake with crack, easy	1.0	3.0	59.1 ± 0.1
3	Brown cake, homogenous, easy	0.5	0.9	61.4 ± 0.1
5	Brown cake, homogenous, easy	0.7	1.3	71.2 ± 0.2

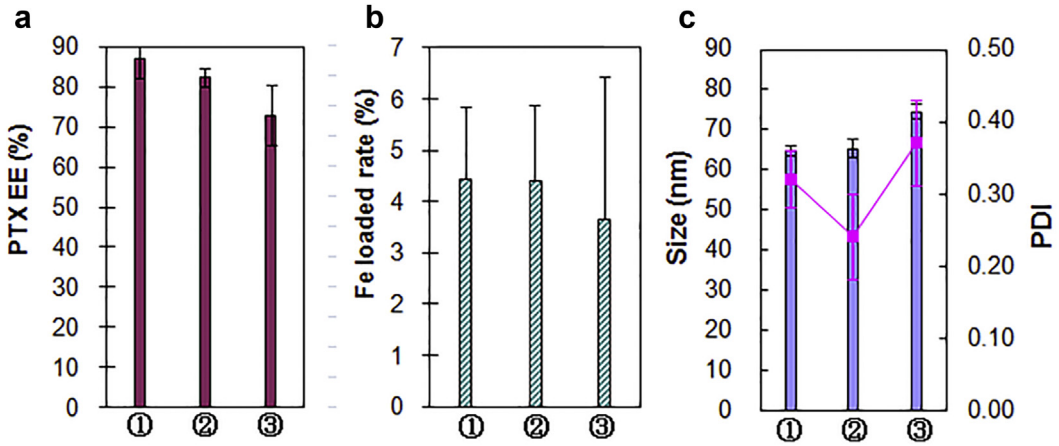

Figure 2. Effect of different molecular weight of PLO on PTX-MNPs, among which, ①, ②, and ③ represented the PTX-MNPs-PLO$_{1000}$, PTX-MNPs-PLO$_{2000}$, PTX-MNPs-PLO$_{4000}$, respectively. (a) EE% of PTX, (b) loaded content rate of Fe, (c) the particle size (column) and PDI (line). (Particle size: PTX-MNPs-PLO$_{1000}$ vs. PTX-MNPs-PLO$_{4000}$, $p < 0.05$, PTX-MNPs-PLO$_{2000}$ vs. PTX-MNPs-PLO$_{4000}$, $p < 0.05$).

agent. Concentration of mannitol (0%, 1%, 3%, and 5%, w/v) was investigated, and distilled water was used as the resuspended dispersion medium. Concentrations of Fe and encapsulated PTX were determined after membrane filtration (0.22 μm). Leaking rates of Fe or PTX, equation listed herewith, were calculated to evaluate the formulation.

$$\text{Leaking rate(Fe)} = \left(1 - C_{\text{Fe},1}/C_{\text{Fe},2}\right) \times 100\% \quad (1)$$

$$\text{Leaking rate(PTX)} = \left(1 - C_{\text{PTX},1}/C_{\text{PTX},2}\right) \times 100\%\,, \quad (2)$$

where C_1 and C_2 were reconstitution before and after.

Characterization of PTX-MNPs-PLO

The Fe concentrations of PTX-MNPs-PLO were measured with a classical C-A (absorbance vs. Fe concentration) calibration curve, which was established with the 1,10-phenanthroline spectrophotometric method on the UV-visible spectrophotometer (UV-3600; Shimadzu).[16] And the loading rate of Fe was calculated by Equation 3.

The entrapment efficiency (EE%) of PTX was obtained by determination of the content encapsulated in MNPs (Eq. 4). Briefly, 5.0 mg of solid PTX-MNPs-PLO was dissolved in 10 mL of methanol under ultrasound, and the nonsoluble Fe_3O_4 NPs were removed through magnetic separation. Then, the supernatant was centrifugated at 10,000 rpm for 10 min. After that, supernatant was next determined by HPLC method, which had the limit of quantification for PTX as 0.04-8.00 μg/mL, and was based on the following experimental conditions: Lichrosphere C18 column (150 × 46 mm i.d.; pore size, 5 μm), the mobile phase: CH_3OH:H_2O (78:28, v/v), flow rate: 1.0 mL/min, and measured wavelength: 227 nm, which had been verified.

$$\text{Loading rate of Fe}(\%) = C_{\text{Fe}}V \Big/ \left(C_{\text{Fe}}V + W_{\text{polymer}}\right) \times 100\% \quad (3)$$

$$\text{EE\% of PTX} = C_{\text{PTX}}V/W_{\text{PTX}} \times 100\%\,, \quad (4)$$

where C_{Fe}, C_{PTX}, and V meant the concentration of Fe in dispersion and the volume of dispersion, whereas W_{polymer} and W_{PTX} stood for the added polymer and PTX weights.

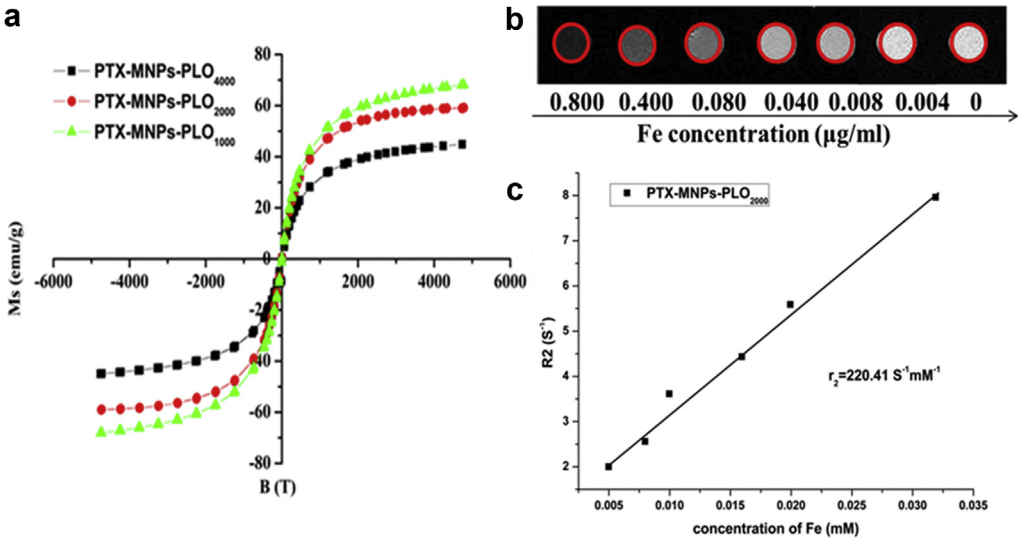

Figure 3. (a) Hysteresis loops for PTX-MNPs-PLO$_{1000}$, PTX-MNPs-PLO$_{2000}$, and PTX-MNPs-PLO$_{4000}$; MRI properties of PTX-MNPs-PLO$_{2000}$. (b) Signal intensity–weighted images (TR = 2500 ms; TE = 10 ms) of MNPs in 1% agarose solution at various iron concentrations at room temperature. Blank agarose solution was taken as a control. (c) Changes of T_2 relaxation rate (R_2) of MNPs as iron concentration increased.

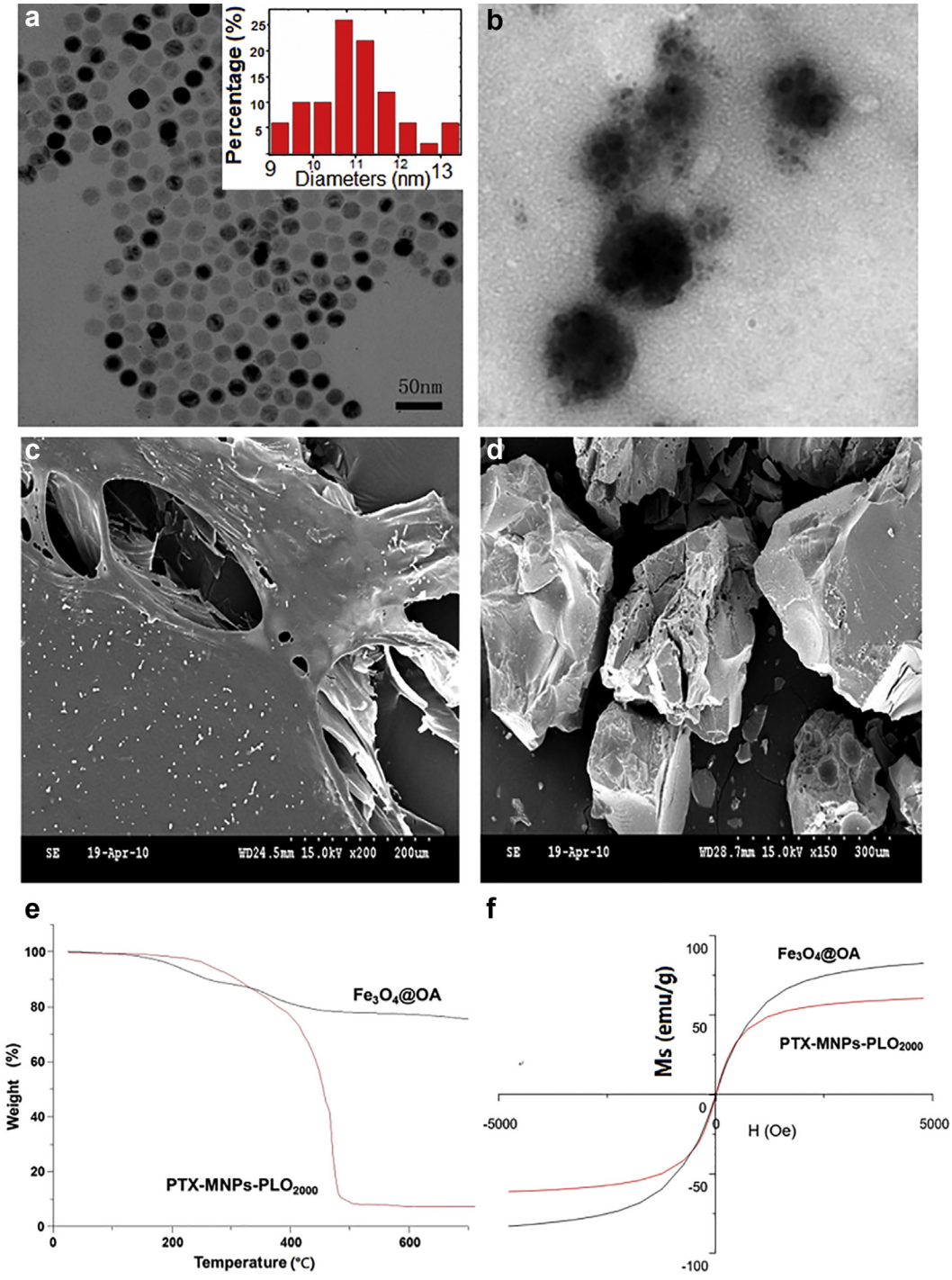

Figure 4. (a and b) Transmission electron microscopy images of Fe_3O_4@OA and PTX-MNPs-PLO_{2000}, respectively, whereas (c and d) represented SEM images of PTX-MNPs-PLO_{2000} and Fe_3O_4@OA in sequence. (e) The TGA of Fe_3O_4@OA and PTX-MNPs-PLO_{2000}. (f) The VSM of Fe_3O_4@OA and PTX-MNPs-PLO_{2000}.

The morphology of the PTX-MNPs-PLO was observed by transmission electron microscope using JEM-2100 (Jeol, Tokyo, Japan). The scanning electron microscopy (SEM) was used to identify the microstructure at S4800 microscope (Hitachi, Tokyo, Japan). The size by intensity and polydispersion index (PDI) were determined by Zeta-sizer Nano ZS90 (Malvern, UK). The thermal behavior of the powders was tested by thermal gravimetric analysis (TGA) using a TGA 7 Thermogravimetric Analyzer (Perkin-Elmer, Waltham, MA) in synthetic N_2 atmosphere up to 700°C with a heating rate of 10°C/min.

The Fe_3O_4@OA and PTX-MNPs-PLO_{2000} were then analyzed by X-ray diffraction (XRD) and Fourier transform infrared spectoscopy (FT-IR) (Nicolet Impact 410; Nicolet Instrument Corporation, Madison, WI). XRD was performed on a Philips MPD 1880 X-ray diffractometer. The diffracted intensity of Cu K_α radiation (40 kV and 40 mA) was measured in a 2θ range between 20° and 70° at a scan speed of 8.0 degree/min and a step size of 0.02°. As for test in FT-IR, samples were mixed with KBr and pressed to get the IR test.

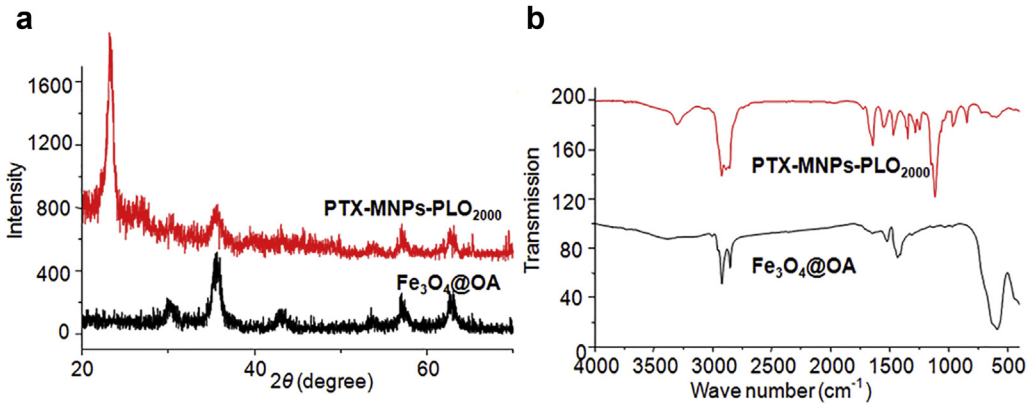

Figure 5. Results of (a) XRD and (b) FT-IR.

Magnetic Properties of PTX-MNPs-PLO

Magnetization measurements were carried out with a Lakeshore 7407 vibrating sample magnetometer (VSM). To evaluate the potential in clinical MRI, the PTX-MNPs-PLO_{2000} suspension was diluted with 1% agarose tubes to a series of solutions containing Fe 0.004, 0.008, 0.04, 0.08, 0.4, and 0.8 μg/mL in an Eppendorf tube, respectively. Mixture of 0.5 mL of distilled water and 1% agarose was designed as the control. MRI was performed at 1.5 T (Siemens Ananto1.5 T System) for T_2-weighted imaging (T_2WI) by using a fast spin-echo sequence (repetition time/echo time [TR/TE], 5500 ms/101 ms; field of view [FOV], 14 × 14 cm; slice thickness, 1.5 cm; and matrix, 384 × 256) and a 16-echo sequence (TR/TE, 3000/22 ms, 44, 66, 88, 110 … 352 ms; FOV, 14 × 14 cm; slice thickness, 1.5 cm; and matrix, 384 × 256) at room temperature. The signal intensities were determined from a circular 20 cm^2 region of interest. The relaxivity coefficient (r_2) as a standardized contrast enhancement indicator was calculated as the gradient of the plot of R_2 ($R_2 = 1/T_2$) versus the molarity of magnetic atoms.

Pharmacokinetics

Male rats ($n = 12$) weighted 200 g were randomly divided into 4 groups ($n = 3$) and injected intravenously through tail vein with PTX-MNPs-PLO_{1000}, PTX-MNPs-PLO_{2000}, PTX-MNPs-PLO_{4000}, and Taxol at the dose of 10 mg of PTX/kg, respectively. In each group, rats were blooded from vein behind the eyeball via glass capillary at 0.083, 0.25, 0.5, 1, 2, 4, or 8 h after drug administration. The blood samples were centrifuged (3000 r/min, 15 min), and PTX was extracted using acetonitrile. The concentration of PTX in the blood was measured by the HPLC assay as described previously, which was verified.

Biodistributions Under Low Magnetic Fields

Male mice ($n = 45$) weighted 15-20 g were randomly assigned to 3 groups ($n = 15$) and injected intravenously through the tail vein with PTX-MNPs-PLO_{2000} (10 mg of PTX/kg) and were followed by placing under 0, 0.6, and 1.2 T permanent magnetic field around the right kidney, respectively. In each group, mice were blooded by cutting the eyeball and sacrificed at 0.25, 0.5, 1, 2, or 4 h after drug administration ($n = 3$ at each time point). The tissue samples, including liver, left kidney, and right kidney, were dissected out. To determine the amount of drug accumulation, organs were weighed and homogenized in 0.5 mL of saline solution per 100 mg of tissue. About 300 μL of acetonitrile were added to the homogenate and vortexed for 3 min. After centrifugation at 16,000 rpm for 10 min, the supernatant was determined by HPLC, demonstrated to be a reliable technique in each tissue including blood.

Results and Discussions

Optimal Process of Preparing the Lyophilized PTX-MNPs-PLO

Three criteria were selected to prompt optimization of preparing loading rate of Fe(%), EE% of PTX, and particle size of PTX-MNPs-PLO. The optimal process was synthetically defined as follows: 110 mg of PLO and 2 mg of PTX were added into the solution of 10 mg of MNPs in 3 mL of THF. The mixture was dropped through a syringe with a thin pinhead into 7 mL of distilled water under agitation and then intermittently ultrasounded with probe for 6 min. Then, the organic solvent was removed and lyophilized to dryness. Effects of different amounts of mannitol on PTX-MNPs-PLO were investigated, and results were displayed in Table 1. The added lyoprotectant could improve the performance; however, an obvious crack could be seen when mannitol was 1%. Compared with group of 5%, the lyophilized powder of 3% mannitol possessed the lowest leakage rate and small particle size. Thus, 3% (w/v) mannitol was selected as the protectant. So, the ultimate formulation could be used after reconstruction by distilled water. Dosage would be determined on concentration of Fe or PTX.

Optimization of Molecular Weight of PLO In Vitro

Different molecular weights of PLO were used to prepare PTX-MNPs-PLO according to the optimized procedure. Loading content of Fe, EE% of PTX, particle size, and saturation magnetization (M_s) of the PTX-MNPs-PLO were selected as the evaluation indexes to

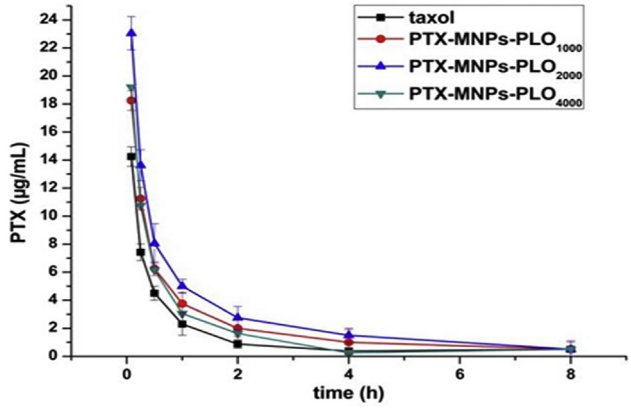

Figure 6. Plasma concentration-time profiles in rats after intravenous administration ($n = 3$).

obtain the right molecular weight. The results were shown in Figures 2 and 3. As we can see from Figure 2, content of Fe and EE% of PTX were both in the order of PTX-MNPs-PLO_{1000} >PTX-MNPs-PLO_{2000} >PTX-MNPs-PLO_{4000}, whereas particle size was in the reverse, which was PTX-MNPs-PLO_{1000} <PTX-MNPs-PLO_{2000} <PTX-MNPs-PLO_{4000} (particle size: PTX-MNPs-PLO_{1000} vs. PTX-MNPs-PLO_{4000}, $p < 0.05$; PTX-MNPs-PLO_{2000} vs. PTX-MNPs-PLO_{4000}, $p < 0.05$), which may be due to the length of hydrophilic group. The higher molecular weight of PLO and the higher hydrophilicity result in decreased account of lipophilic groups; therefore, the drug loading capacity of lipophilic drugs was decreased.

Figure 3a showed the M_s of PTX-MNPs-PLO, which was obtained using VSM at room temperature (300 K). As shown in Figure 3a, the hysteresis loops showed negligible residual magnetization and essentially no coercivity for all PTX-MNPs-PLOs, indicating their remarkable superparamagnetism. It could refer that modification of PLO could not change the superparamagnetism of Fe_3O_4@OA. However, the M_s was decreased as the molecular weight increased, which may attribute to the increasing amount of nonmagnetic materials.

Also, as we know, the high value of M_s leads to enhanced MRI contrast effect.[17] Specifically, we evaluated the T_2WI MRI contrast effect of PTX-MNPs-PLO_{2000}. As shown in Figures 3b and 3c, the samples displayed a clear concentration-dependent T_2 signal reduction effect, which was shown by the MR contrast changing from light gray to black as the concentration of PTX-MNPs-PLO_{2000} increased. Image gray was set as the control when Fe concentration was 0. The corresponding relaxivity coefficient (r_2) value of 220.41 $mM^{-1}s^{-1}$ was obtained by calculation of the plot of R_2 versus the molarity of Fe.

Characterization of PTX-MNPs-PLO_{2000}

Results of comparison characterization of Fe_3O_4@OA and PTX-MNPs-PLO_{2000} were displayed in Figures 4a and 4b representing transmission electron microscopy images of Fe3O4@OA and PTX-MNPs-PLO2000, respectively. From Figure 4a, we can see that the particles of Fe_3O_4@OA were monodispersed, and the average core particle size was about 20 nm. Figure 4b showed small clusters, less than 100 nm, which indicated that the magnetic cores were successfully modified with PLO_{2000}. The SEM images of PTX-MNPs-PLO_{2000} and Fe_3O_4@OA were shown in Figures 4c and 4d in sequence, which were found in the flocculent and porous surfaces; accordingly, the lyophilized PTX-MNPs-PLO_{2000} powders possessed desirable reconstruction capability.

TGA was measured under the protection of N_2 aiming to confirm the formation and evaluate the binding efficiency. As shown in Figure 4e, there kept a slight weight loss till to about 250°C, possibly due to the evaporation of water, whereas a clear weight loss when above 250°C in both curves. When above 250°C, the weight loss in group of Fe_3O_4@OA might attribute to decomposition of OA, which was composed into monolayer as the particle surface, whereas the sharp weight loss of PTX-MNPs-PLO might be due to the decomposition of PLO_{2000}. And it could also be calculated to get the content of PLO in MNP, which was about 70%. Figure 4f displayed the VSM results of Fe_3O_4@OA and PTX-MNPs-PLO_{2000}; it further could be seen that the M_s of PTX-MNPs-PLO_{2000} was about 70% of that of Fe_3O_4@OA, which would infer that the polymer did not have an effect on the magnetic saturation of the MNPs.

Figure 5a shows the results of XRD. Diffraction peak of Fe_3O_4@OA and PTX-MNPs-PLO_{2000} was consistent with that of Fe_3O_4 indicating that the preparations did not change the spinel structure of Fe_3O_4. And when 2θ ranged from 20° to 30°, a strong peak existed in PTX-MNPs-PLO_{2000}, which sorted of amorphous phase and might owe to the amorphous phase PTX and PLO_{2000}. PTX accounted in a very low amount in the formulation and reported no characteristic peak from 20° to 30°.[18] Thus, a peak at c.a. 22θ for PTX-MNPs-PLO might attribute to the PLO. Figure 5b displayed the results of FT-IR; the high absorption at 563.4 cm^{-1} indicated the Fe-O, and 1111 cm^{-1} represented the -CH_2-O-CH_2- of PLO_{2000}, which demonstrated that the PLO_{2000} was modified into the surface of Fe_3O_4@OA.

Pharmacokinetics

Figure 6 displayed the PTX concentration obtained from HPLC at desired time, and 3P97 software (Chinese Pharmacological Society, Beijing, China) was used to identify the mimic compartment model to get the pharmacokinetic parameters, which are shown in Table 2. It was found that the area under the curve (AUC) values were in order of PTX-MNPs-PLO_{2000} >PTX-MNPs-PLO_{1000} >PTX-MNPs-PLO_{4000} >Taxol (particles vs. free drug, $p < 0.05$), indicating the enhanced drug bioavailability in the delivery systems of NPs. PTX-MNPs-PLO_{2000} was cleared from blood most slowly among all samples, indicating that the PLO especially PLO_{2000} could benefit to prolong blood circulation time of the PTX-MNPs, probably due to the shielding effect of the PLO. For various PTX-MNPs-PLO, the AUC value of PTX-MNPs-PLO_{2000} was higher than that of PTX-MNPs-PLO_{1000}, which probably owed to the higher PEG molecular weight. Stronger hydrophilic property possessed by PLO_{2000} resulted in increased shield effect. It was also higher than that of PTX-MNPs-PLO_{4000} possibly because of the redundant hydrophilicity of PLO_{4000}. Emulsion stability was consequently destroyed, and entrapment rate of PTX was accordingly deduced.[19] Thus, the balance between PEGylation and the lipophilic group in one formulation was an important factor influencing the blood circulation lifetime of PTX-MNPs. Thus, the PTX-MNPs-PLO_{2000} should have more potential in cancer therapy.

Biodistribution

Once the PTX-MNPs-PLO_{2000} was selected, information could be collected: PTX EE% = (82.6 ± 2.3)%, Fe loaded rate% = (4.4 ± 1.5)%,

Table 2
Main Pharmacokinetics Parameters of PTX After Intravenous Administration of Taxol, PTX-MNPs-PLO_{1000}, PTX-MNPs-PLO_{2000}, and PTX-MNPs-PLO_{4000} to Rats (Mean ± SD; $n = 3$)

Parameters	Taxol	PTX-MNPs-PLO_{1000}	PTX-MNPs-PLO_{2000}	PTX-MNPs-PLO_{4000}
AUC (μg mL^{-1} h)	11.406 ± 2.474	19.571 ± 3.203[a,b]	26.923 ± 6.09[a,b,c]	16.692 ± 2.300[a]
MRT (h)	1.022 ± 0.245	1.617 ± 0.744	1.980 ± 0.625	1.260 ± 0.371
Vd (L kg^{-1})	0.559 ± 0.258	0.271 ± 0.068	0.208 ± 0.025	0.306 ± 0.060
CL (L kg^{-1} h^{-1})	0.541 ± 0.105	0.312 ± 0.050	0.233 ± 0.056	0.364 ± 0.051
$t_{1/2\alpha}$ (h)	0.435 ± 0.235	0.194 ± 0.062	0.187 ± 0.078	0.269 ± 0.083
$t_{1/2\beta}$ (h)	1.899 ± 1.762	2.158 ± 1.049	2.103 ± 0.676	1.757 ± 0.183

MRT, mean residence time; Vd, volume of distribution; CL, systemic clearance.
[a] Significantly different from Taxol ($p < 0.05$).
[b] Significantly different from PTX-MNPs-PLO_{4000} ($p < 0.05$).
[c] Significantly different from PTX-MNPs-PLO_{1000} ($p < 0.05$).

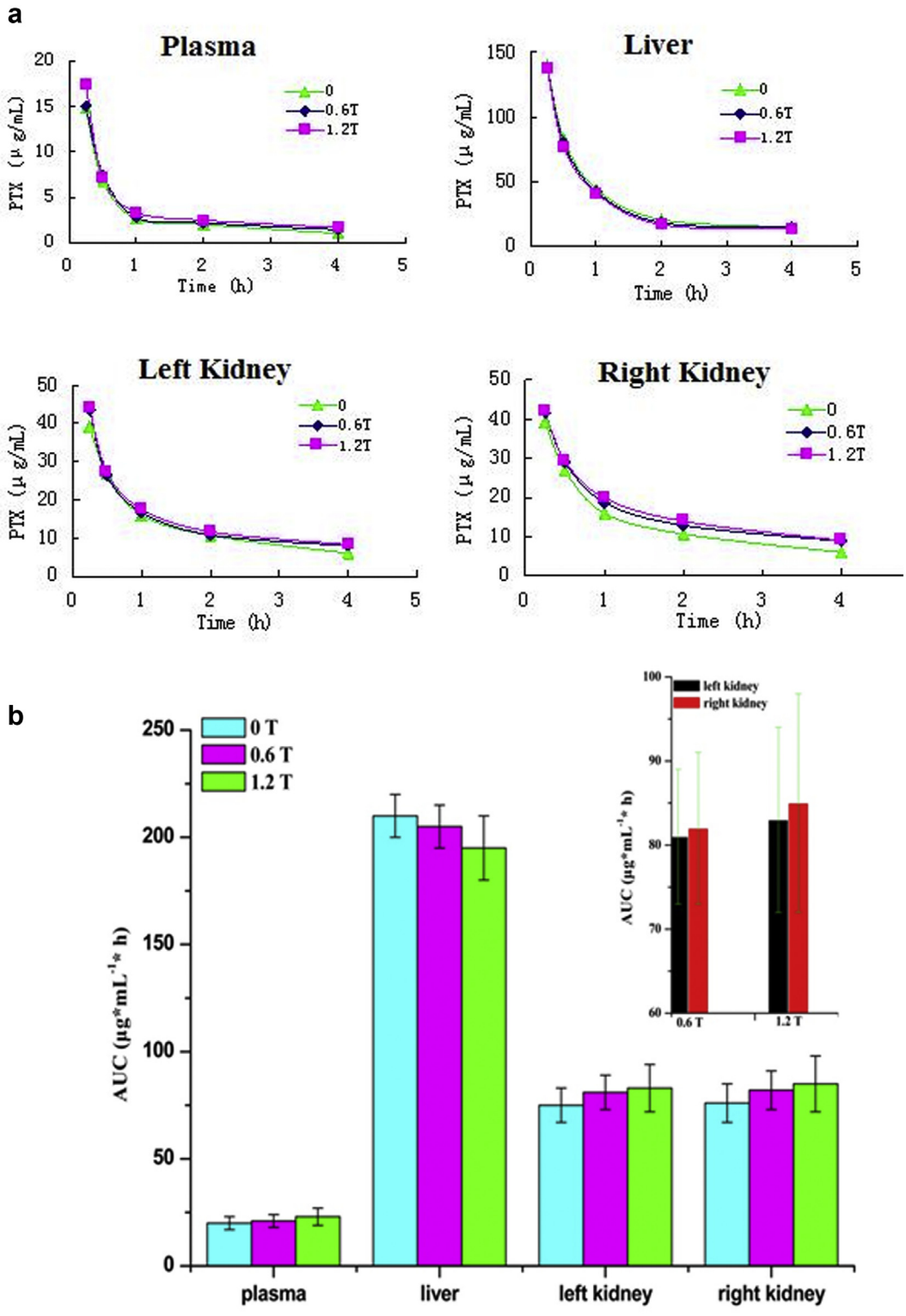

Figure 7. (a) The concentration-time curves of PTX in tissues of mice given PTX-MNPs-PLO$_{2000}$ after intravenous administration in different magnetic fields. (b) Comparison of AUC of PTX tissues of mice given PTX-MNPs-PLO$_{2000}$ after intravenous administration in different magnetic fields. All the magnetic intensities were assigned at 0, 0.6, and 1.2 T. No significant difference between left and right kidneys under both 0.6 and 1.2 T ($p > 0.05$).

hydrodynamic size = 65.3 ± 2.3 nm, and PDI = 0.24 ± 0.06. Next, biodistribution of PTX-MNPs-PLO$_{2000}$ in mice was determined at 0.25, 0.5, 1, 2, or 4 h after injection. The concentration-time curves of PTX in plasma and tissues were presented in Figure 7a, and the corresponding AUC at 4 h was calculated and displayed in Figure 7b. From that, we could see PTX was present in particularly high levels in liver after injection. The accumulation of PTX in liver was influenced by the additional magnetic field, and the AUC value in this tissue was in the order of 0 T > 0.6 T > 1.2 T, whereas AUC in plasma or kidneys including left and right was 1.2 T > 0.6 T > 0 T, suggesting

that the additional magnetic field around kidney had the trends in reducing phagocytosis by liver and in increasing distribution in kidney. However, there was no significant difference between each magnetic field, 0.6 or 1.2 T, $p > 0.05$. Under the same magnetic field, the AUC of the right targeted kidney was slightly higher than that of the left kidney, yet with no significant difference ($p > 0.05$, shown in Fig. 7b). These results indicated that low magnetic field intensity outside the body (such as 0.6 and 1.2 T) was almost helpless for drug-loaded magnetic particles accumulation if the targeting region was inside deeply, probably due to the decrease in magnetic intensity at the increased distance between the polar and target tissue. The current targeted strategy may only suit for the body surface lesions. Or, that promising deeply buried magnetic field would hold out hope of better targeted accumulation in kidneys.[20]

Conclusions

In the present research, we had modified MNPs with PLO as the carrier of PTX, which would improve the long time circulating and biocompatibility. The long circulation lifetime of PTX-MNPs-PLO_{2000} was acquired compared with Taxol, PTX-MNPs-PLO_{1000}, and PTX-MNPs-PLO_{4000}. And the results exhibited that PTX-MNPs-PLO_{2000} maintained the superparamagnetic property, which would benefit to magnetic accumulation, target drug delivery, and thermal therapy. Based on the discussion, magnetic targeting application might confine at the body surface lesion, or else suggestions of magnetic targeting therapy of kidneys likely refer to preferable deep-seated magnet.

Acknowledgments

This work was financially supported by National Natural Science Foundation of China (81473160), the Basic Research Program of Jiangsu Province (Natural Science Foundation, no. BK20151422), Fundamental Research Funds for the Central Universities (2242014R30013 and 2242016K40033), and Scientific and Technological Project of Zhenjiang (no. SS2015023).

References

1. Schleich N, Sibret P, Danhier P, et al. Dual anticancer drug/superparamagnetic iron oxide-loaded PLGA-based nanoparticles for cancer therapy and magnetic resonance imaging. *Int J Pharm*. 2013;447(1-2):94-101.
2. Cunningham CH, Arai T, Yang PC, McConnell MV, Pauly JM, Conolly SM. Positive contrast magnetic resonance imaging of cells labeled with magnetic nanoparticles. *Magn Reson Med*. 2005;53(5):999-1005.
3. Johannsen M, Gneveckow U, Eckelt L, et al. Clinical hyperthermia of prostate cancer using magnetic nanoparticles: presentation of a new interstitial technique. *Int J Hyperthermia*. 2005;21(7):637-647.
4. Purushotham S, Ramanujan RV. Thermoresponsive magnetic composite nanomaterials for multimodal cancer therapy. *Acta Biomater*. 2010;6(2):502-510.
5. Gupta AK, Gupta M. Synthesis and surface engineering of iron oxide nanoparticles for biomedical applications. *Biomaterial*. 2005;26:3995-4021.
6. Hosmer JM, Shin SH, Nornoo A, Zheng H, Lopes LB. Influence of internal structure and composition of liquid crystalline phases on topical delivery of paclitaxel. *J Pharm Sci*. 2011;100:1444-1455.
7. Weiszhár Z, Czúcz J, Révész C, Rosivall L, Szebeni J, Rozsnyay Z. Complement activation by polyethoxylated pharmaceutical surfactants: Cremophor-EL, Tween-80 and Tween-20. *Eur J Pharm Sci*. 2012;45(4):492-498.
8. Xie J, Xu C, Kohler N, Hou Y, Sun S. Controlled PEGylation of monodisperse Fe_3O_4 nanoparticles for reduced non-specific uptake by macrophage cells. *Adv Mater*. 2007;19(20):3163-3166.
9. Kolate A, Baradia D, Patil S, Vhora I, Kore G, Misra A. PEG—a versatile conjugating ligand for drugs and drug delivery systems. *J Control Release*. 2014;192:67-81.
10. Gref R, Lück M, Quellec P, et al. 'Stealth' corona-core nanoparticles surface modified by polyethylene glycol (PEG): influences of the corona (PEG chain length and surface density) and of the core composition on phagocytic uptake and plasma protein adsorption. *Colloids Surf B Biointerfaces*. 2000;18(3-4):301-313.
11. Arruebo M, Fernández-Pacheco R, Ibarra MR, Santamaría J. Magnetic nanoparticles for drug delivery. *Nano Today*. 2007;2(3):22-32.
12. Zhou LJ, Liu JP, Xiong F, Chen YJ, Huang RR, Gu N. Preparation and in vitro evaluation of PEG-coated superparamagnetic iron oxide nanoparticles. *J China Pharm Univ*. 2013;44(4):316-320.
13. Chen YJ, Tao J, Xiong F, et al. Synthesis, self-assembly, and characterization of PEG-coated iron oxide nanoparticles as potential MRI contrast agent. *Drug Dev Ind Pharm*. 2010;36(10):1235-1244.
14. Song L, Zang F, Song M, Chen G, Zhang Y, Gu N. Effective PEGylation of Fe3O4 nanomicelles for in vivo MR imaging. *J Nanosci Nanotech*. 2015;15(6):4111-4118.
15. Liu SF, Xu AX, Yuan QH, Liu SK. Studies on the preparation and in vitro release characteristics of Flurbiprofen (poly lactic-co-glycolic acid) microspheres for intra-articular injection. *J Pharm Res*. 2015;34(2):87-90.
16. Xie J, Yan C, Zhang Y, Gu N. Shape evolution of "multibranched" Mn–Zn Ferrite nanostructures with high performance: a transformation of nanocrystals into nanoclusters. *Chem Mater*. 2013;25(18):3702-3709.
17. Xie J, Zhang Y, Yan C, et al. High-performance PEGylated Mn–Zn ferrite nanocrystals as a passive-targeted agent for magnetically induced cancer theranostics. *Biomaterial*. 2014;35(33):9126-9136.
18. Patel K, Patil A, Mehta M, Gota V, Vavia P. Oral delivery of paclitaxel nanocrystal (PNC) with a dual Pgp-CYP3A4 inhibitor: preparation, characterization and antitumor activity. *Int J Pharm*. 2014;472:214-223.
19. Ferrara KW, Borden MA, Zhang H. Lipid-shelled vehicles: engineering for ultrasound molecular imaging and drug delivery. *Acc Chem Res*. 2009;42(7):881-892.
20. Kubo T, Sugita T, Shimose S, Nitta Y, Ikuta Y, Murakami T. Targeted systemic chemotherapy using magnetic liposomes with incorporated adriamycin for osteosarcoma in hamsters. *Int J Oncol*. 2001;18(1):121-125.